

Informal Documentation

**Initial Testing of the New Ex-Core Fast Neutron Irradiator
at the UMass-Lowell Research Reactor**

**Dr. John R. White
Chemical and Nuclear Engineering Department**

and

**Leo Bobek and Thomas Regan
Radiation Laboratory**

**University of Massachusetts Lowell
Lowell, MA 01854**

June 18, 2002

Initial Testing of the New Ex-Core Fast Neutron Irradiator at the UMass-Lowell Research Reactor

John R. White, Professor, Chemical and Nuclear Engineering Department
and

Leo Bobek, Reactor Supervisor, Radiation Laboratory
Thomas Regan, Reactor Engineer, Radiation Laboratory

University of Massachusetts Lowell
Lowell, MA 01854

June 18, 2002

Introduction

A new ex-core fast neutron irradiation (FNI) facility has recently been installed within the pool of the University of Massachusetts Lowell Research Reactor (UMLRR). This new experimental facility replaces the three beam ports that originally existed on one side of the core. It was designed to give a fast flux level $\geq 10^{11}$ n/cm²-s, with relatively low thermal fluence and gamma dose rates. Samples with a cross-sectional area as large as 12"x12" and up to 6" thick can be irradiated within the new facility. The fast neutron flux was designed to be nearly uniform over the 12"x12" area facing the core, and the fast fluence variation through the sample thickness is minimized via a single 180° rotation of the sample canister at the midpoint of the irradiation period. This new fast neutron irradiation (FNI) facility offers a significantly larger sample volume than previously available within the Radiation Laboratory at UMass-Lowell.

A recent paper¹ describes the design philosophy and final geometry configuration for the FNI in some detail and it presents summary results from a series of 2-D VENTURE² and DORT³ models for the complete facility. In particular, Ref. 1 gives a detailed description of the as-built modular FNI arrangement, including the sample canister, shield elements, four aluminum blocks, large Al guide collar, and the single flux-shaping element -- which all fit within the large grid structure just to the side of the core. It also describes the in-core changes that were needed to optimize the performance of the new FNI facility, including the replacement of five graphite reflector elements nearest to the FNI with five leaded-void boxes, and the movement of the centrally located partial fuel elements towards the core periphery to offset the negative reactivity associated with the addition of the Pb-void assemblies.

The overall computational methodology and many of the results of the design calculations using a variety of XY and YZ VENTURE and DORT models are also reported in Ref. 1. The computer modeling was used to guide the design process and to show that the final FNI design did indeed meet the initial quantitative design specifications imposed upon the new experimental facility. In particular, the somewhat simplified computational models (simplified in the context of the 3-D to 2-D approximation that was required) showed that the new FNI

- can support experimental samples as large as 12"x12"x6",
- does have a fast flux and 1 MeV equivalent flux $\geq 10^{11}$ n/cm²-s,

- has a better than 20:1 fast-to-thermal flux ratio and a total gamma dose rate to the sample ≤ 100 Krad/hr,
- does achieve a uniform distribution of the fast flux throughout the sample to within $\pm 10\%$ of the average value, and
- does have a maximum reactivity effect that is significantly below the Technical Specification limit for movable experiments in the UMLRR ($0.1 \text{ \%}\Delta k/k$).⁴

However, although our experience with computer modeling for the UMLRR in the past has been quite good⁵⁻⁷, it was understood at the beginning that a full set of experimental tests and validations would be required after the actual construction and installation of the new facility was complete. Clearly the modeling was essential for the design process, but actual experimental evidence would be required to characterize the real performance of the as-built FNI facility. Thus, the goal of this paper is to address the testing phase of this project, including a description of the experimental program that was performed to characterize the FNI, a discussion of the key results of the measurement program, and a review of the comparisons made between computed and experimental results. The documentation presented here gives a basis of key performance indicators for the support of routine operation of the new FNI facility.

The Current UMLRR Configuration and Geometry Orientation

A conceptual sketch of the current UMLRR facility, which highlights the core in the center, the three remaining beam ports at the bottom of the figure, the large graphite reflector on the right, and the general location of the new FNI grid and sample canister at the top, is given in Fig. 1. In the figure, the x coordinate goes from left to right and the y direction goes from top to bottom of the page. The key features in this conceptual sketch can also be seen in Figs. 2a and 2b, which show two views of the actual XY model used to generate many of the computational results to be reported shortly. In addition to the large features mentioned above, one can also identify many of the explicit structures within the core (fuel elements, control blades, leaded-void boxes, etc.), and the explicit components of the new ex-core FNI facility (shield blocks, pure aluminum elements, the flux-shaping element, and the sample and canister regions).

The direction going into the page in Fig. 1 represents the z coordinate, where +z points from the top to the bottom of the reactor. This can be seen explicitly in Figs. 3a and 3b, which show two views of the actual YZ computational geometry. The YZ model also shows explicit zones for the fuel elements, control channels, Pb-void box, shield blocks, flux-shaping filter, and sample canister. In addition, the treatment of the z-direction allows the representation of the upper and lower reflectors, the FNI and core grid boxes, the aluminum guide collar, and the full extent of the sample canister.

These pictures hopefully acquaint the reader with the overall UMLRR core and FNI geometry. Also, in order to appreciate the discussions to follow, it is also important to understand the choice of coordinate system used in the description of the UMLRR. In particular, one should note that the XZ plane is parallel to the right or left face of the FNI canister in Fig. 3b and to the upper and lower faces of the core as shown in Fig. 2b. The y direction cuts perpendicular to the long control blades and through the 9" thickness of the FNI sample canister.

Note: The YZ model in Figs. 3a and 3b differs slightly from that given in Ref. 1. The model given here represents the final YZ computational model, where two zones just below the sample region have a slightly different material composition (to correct an error in the original model).

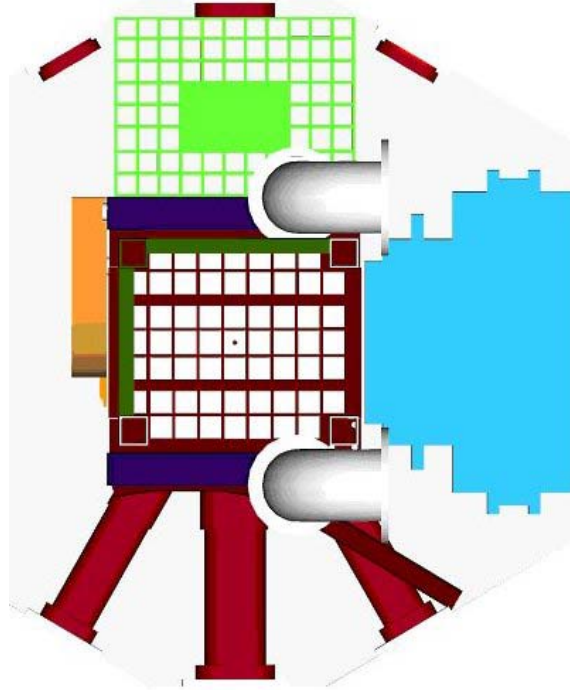


Fig. 1 Conceptual sketch (top view) of the UMLRR with the FNI grid present.

Overview of the Experimental Program

There were several quantities that needed to be measured as part of a comprehensive experimental program. Clearly our initial focus was on characterizing the space and energy distribution of the fast flux within the FNI experimental canister. However, several other experimental parameters, including a measurement of the thermal flux, an estimate of the gamma dose rate, and a test of the reactivity worth associated with movement of the sample canister, were also needed. A series of several preliminary and final tests were made with an empty canister to determine these parameters, including the calibration (or re-calibration) of various measurement techniques along the way. In particular, the final tests reported here include the following measurements for a voided canister:

- I. $^{32}\text{S}(n,p)^{32}\text{P}$ reaction rate measurements to address the uniformity of the fast flux in the plane parallel to the side of the core (XZ plane).
- II. Fast spectrum measurements using a variety of energy-sensitive activation foils to estimate the average 1 MeV equivalent flux within the sample canister.
- III. Miscellaneous measurements to determine the thermal flux, the gamma dose rate, and the reactivity worth associated with the movement of the large FNI sample canister.

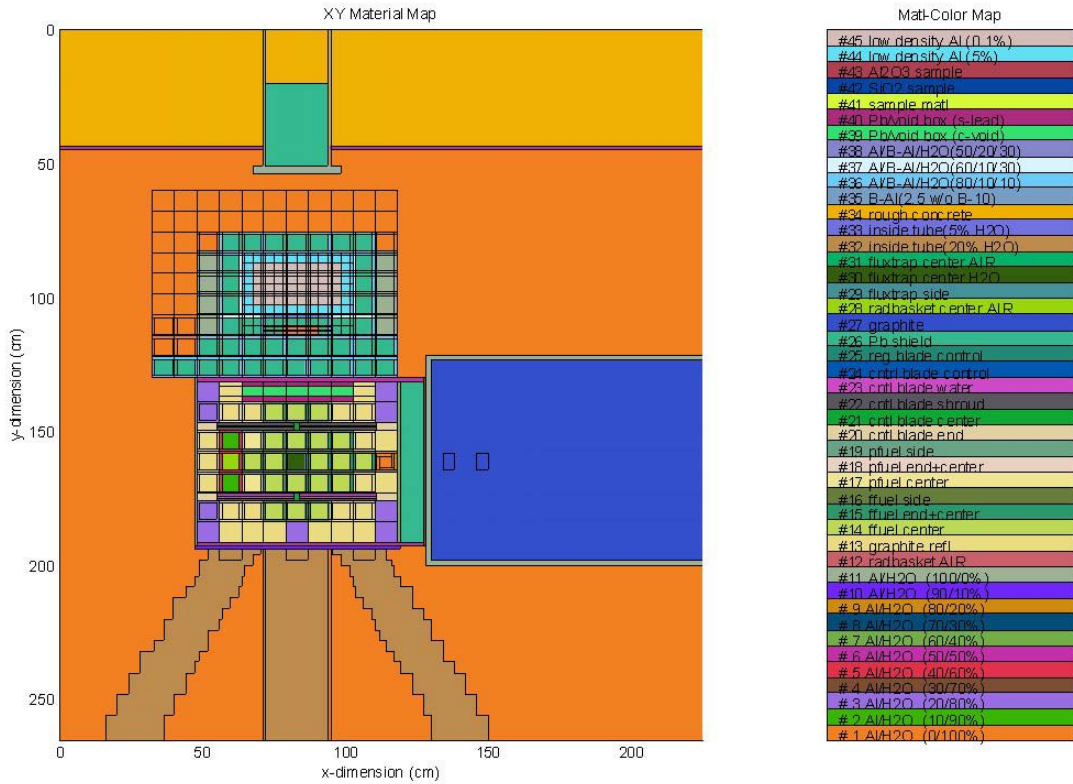


Fig. 2a Full view of XY computational model.

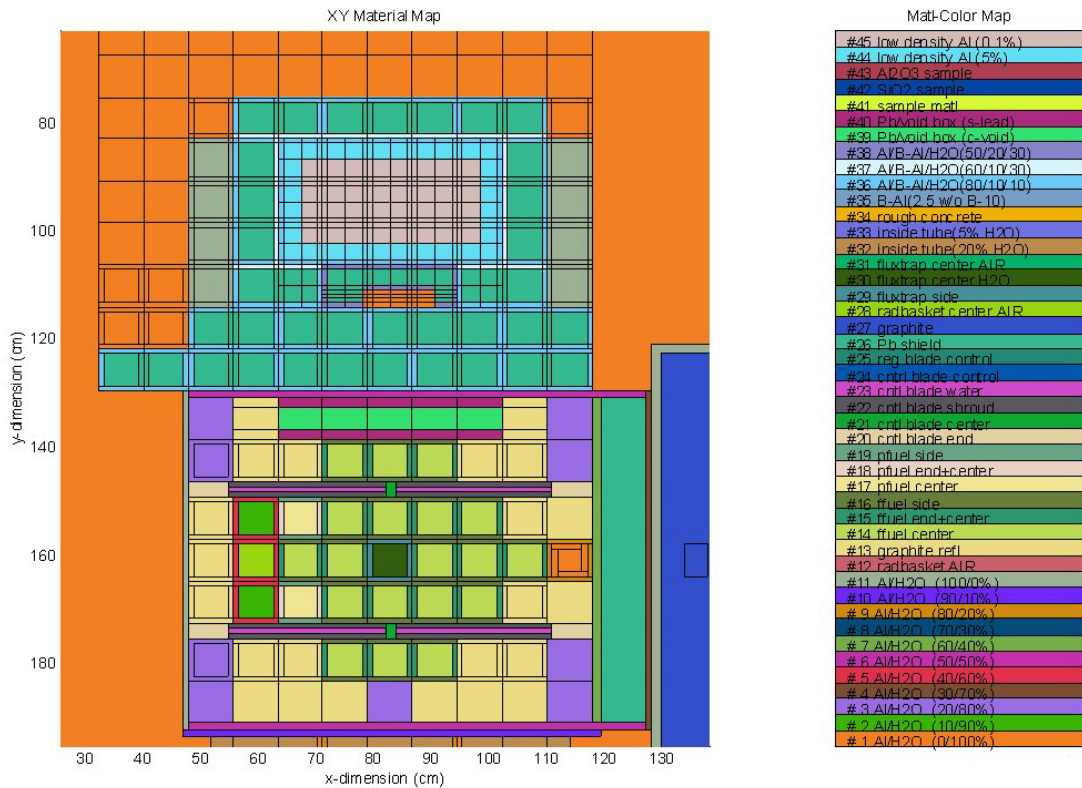


Fig. 2b Expanded view of core and FNI from XY computational model.

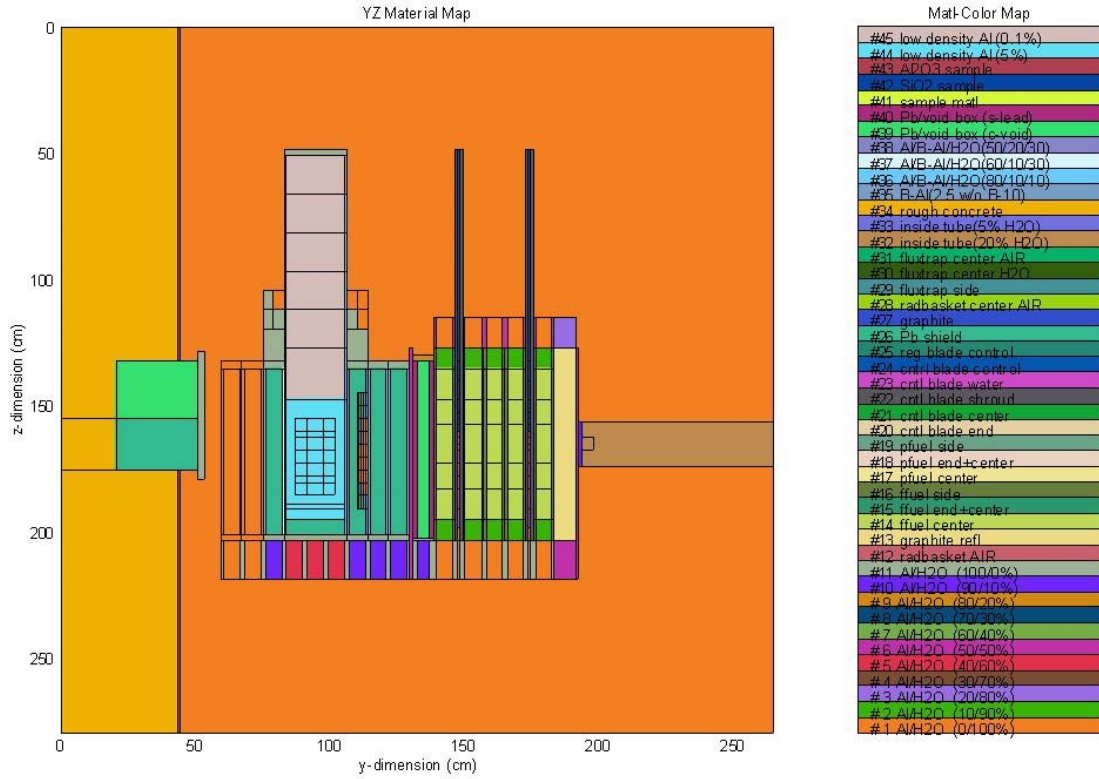


Fig. 3a Full view of final YZ computational model.

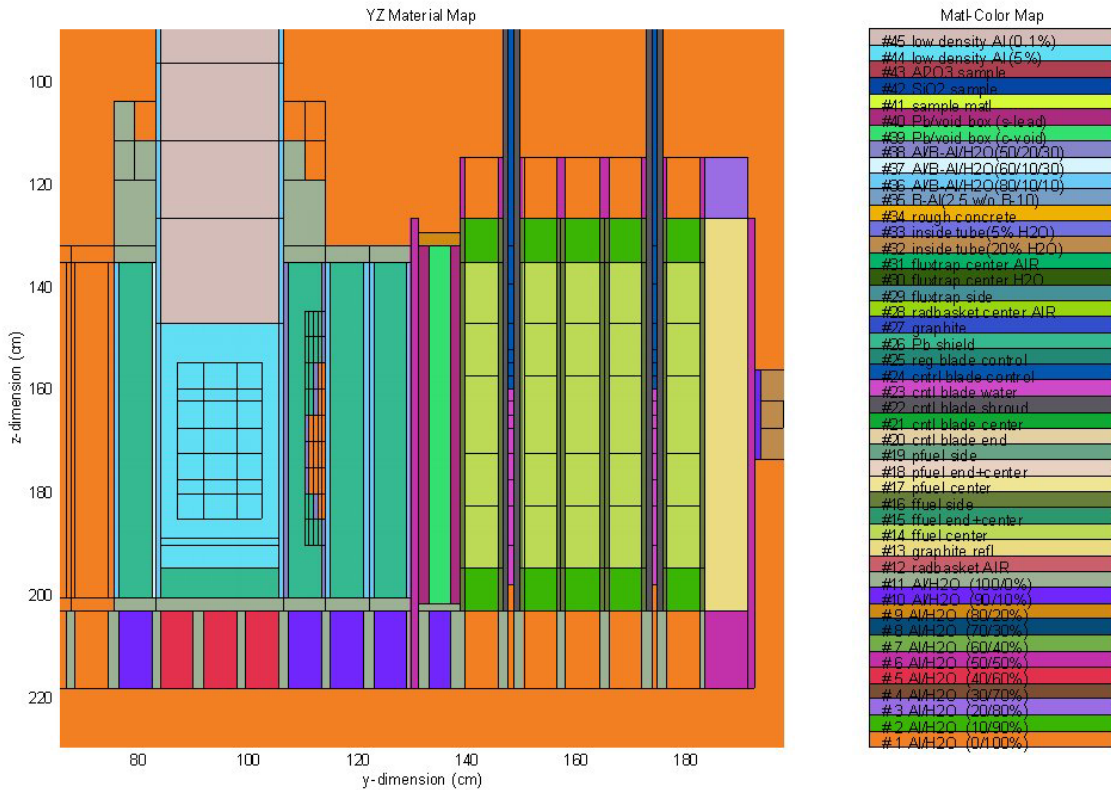


Fig. 3b Expanded view of core and FNI from final YZ computational model.

Note that the characterization of the empty canister will evaluate the reference radiation environment for the new irradiator. We expect that including a sample will only have a minor effect on the spectral characteristics, but it may cause some measurable flux attenuation through the y-direction. Although this attenuation will be minimized by the sample rotation at the mid-irradiation point, each specific sample will be evaluated to assure that the customer-specific uniformity requirements are met.

Each of the tests listed above is addressed separately in the following sections of this paper. Each discussion includes a brief description of the experimental setup, a summary of the measurement results, a critical comparison of the experimental results with those from the analytical computer models and, finally, a summary interpretation and/or rationalization of the overall results within the context of the expected performance of the FNI. Some concluding remarks and several items for further study are also briefly mentioned in the final section of this paper.

Uniformity of the Fast Flux in the XZ Plane

One of the first performance indices to be evaluated was the uniformity of the fast flux in the plane parallel to the face of the core (XZ plane). To experimentally map the fast flux distribution in this plane, a set of 22 sulfur tablets were distributed on the inside front face of the FNI canister as illustrated in Fig. 4. Since planned operation calls for a 180° rotation at the mid irradiation point, a similar distribution of sulfur tabs was also placed on the inside back face of the FNI sample region. Relative to Figs. 2 and 3, the aluminum sheets with the sulfur tabs were hung so that they were positioned near the wall side of the gap between the canister wall and the sample area. Note, however, that there was no sample present for these measurements, since the early tests focused on characterization of the empty canister.

The reactor was operated at 10 kW for one hour, the canister was rotated 180° in the XY plane, and another hour of irradiation was achieved. During irradiation, the ^{32}S n,p reaction produces ^{32}P , which subsequently decays back to ^{32}S by β^- emission with a 14.28 day half-life. The ^{32}P decay rate was measured and the original ^{32}S n,p reaction rate was inferred from the count rate data. A saturated activity with units of reactions per second per atom was then determined and the distribution of this reaction rate is directly proportional to the fast flux level at each measurement point -- because the effective n,p reaction cross section does not change. Since the majority of the ^{32}S n,p reaction occurs in the energy range from about 2 MeV to 7 MeV, studying the ^{32}S n,p distribution gives a direct look at the spatial distribution of the neutrons in this energy range.

The data for the corresponding front-face and back-face sulfur tablets, after accounting for the 180° flip, were averaged to get a single reaction rate value for each of the 22 x,z points measured in this particular experiment. There was a small deviation between the front and back reaction rates (average absolute difference was 3.2%), due primarily to the difficulty associated with exact positioning of the sulfur tablets and to the inherent uncertainty in the counting process. Finally, the average measured reaction rates were normalized to an actual power level of 1 MW, which represents the full power level of the UMLRR. Note that a calibration factor of 0.90 -- which represents the difference between the actual power level and the indicated power level -- was included as part of this final normalization.

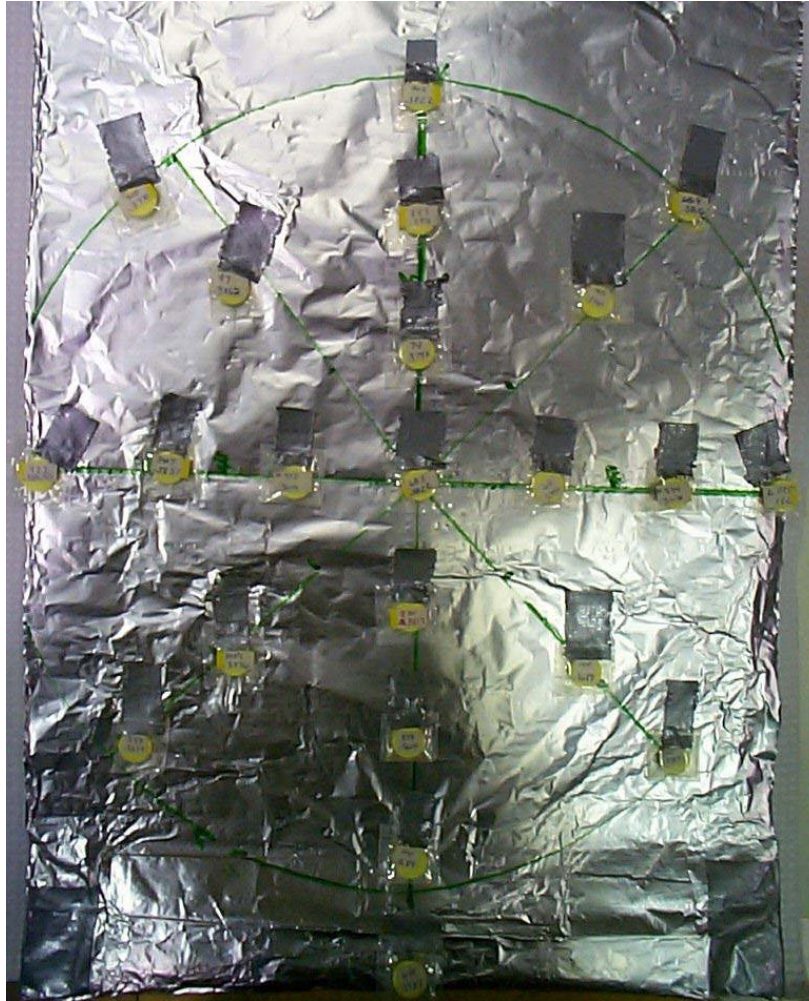


Fig. 4 Location of sulfur tabs on front face of FNI.

The experimental data described above are summarized in tabular form in the first part of Table 1 and in graphical form in Fig. 5. The numerical data have been multiplied by 10^{15} for simplicity, so that the maximum absolute reaction rate at 1 MW operation is about 1.76×10^{-15} reactions per second per atom. Of more interest, however, is the distribution of the reaction rate data relative to the sample center (point #5) as shown in Fig. 5. Here we see a relatively uniform distribution, with a maximum ratio of 1.01 at point #4 and a minimum ratio of 0.81 at point #20, covering an area associated with a 12" diameter circle. Over an 8" diameter circle relative to the sample center at point #5, the maximum to minimum variation is only about 10-11%. Finally, we also note that the ^{32}S n,p profile appears to decrease less rapidly near the bottom of the full sample area relative to the top sample region. This suggests that the sample center could possibly be moved down slightly to achieve an even more uniform reaction rate distribution.

The immediate conclusion from the observed 20% variation in the measured ^{32}S n,p reaction rate over most of the sample area suggests that the desired design goal of a $\pm 10\%$ variation about the average was just barely achieved for neutrons in the 2 MeV – 7 MeV energy range. In addition, the experimental data suggests that the uniformity of the flux profile may be improved somewhat by shifting the sample center slightly towards the lower portion of the XZ plane.

Table 1 Data from ^{32}S n,p distribution measurements and calculations.

Point	X Location	Z Location	Measured RR (rps/atom*10 ¹⁵)	Calculated RR* (rps/atom*10 ¹⁵)	C/E Ratio
1	6.00	-1.75	1.56	1.44	0.92
2	6.00	0.00	1.69	1.56	0.92
3	6.00	2.00	1.72	1.67	0.97
4	6.00	4.00	1.76	1.71	0.97
5	6.00	6.00	1.73	1.72	0.99
6	6.00	8.00	1.67	1.68	1.01
7	6.00	10.00	1.57	1.60	1.02
8	6.00	11.75	1.42	1.50	1.05
9	0.25	6.00	1.47	1.45	0.99
10	2.00	6.00	1.61	1.59	0.99
11	4.00	6.00	1.72	1.67	0.97
12	8.00	6.00	1.73	1.69	0.98
13	10.00	6.00	1.66	1.66	1.00
14	11.75	6.00	1.59	1.58	1.00
15	3.25	3.25	1.68	1.64	0.98
16	3.25	8.75	1.57	1.59	1.02
17	8.75	8.75	1.61	1.62	1.01
18	8.75	3.25	1.73	1.67	0.96
19	1.75	1.75	1.53	1.53	1.00
20	1.75	10.25	1.40	1.46	1.04
21	10.25	10.25	1.49	1.53	1.03
22	10.25	1.75	1.66	1.59	0.96

* The calculated reaction rates given here have already been divided by an average bias of 1.16. This 2-D model normalization was determined from the average C/E ratio calculated for the ^{32}S n,p reaction in the XY DORT model.

To compare to the experimental data, we have also extracted the ^{32}S n,p reaction rate distribution information from the DORT XY and YZ models. Lacking real 3-D information, the calculated XZ distribution was constructed from the appropriately averaged front-face and back-face x-profiles from the XY model and the averaged front and back z-profiles from the YZ model. In particular, a normalized z-profile from the YZ model was used to modulate the x-directed absolute reaction rate data from the XY model. Thus, the computed average reaction rate distribution, $\text{RRc}(x,z)$, for the front-face and back-face y locations is given by

$$\text{RRc}(x,z) = \frac{\text{RR}_{xy}(x)}{1.16} \frac{\text{RR}_{yz}(z)}{\text{RR}_{yz}(z)|_{\text{center}}} \quad (1)$$

The 1.16 bias noted in the above equation was obtained as the average calculated-to-experimental ratio (C/E) for the front and back x-directed profiles at the axial centerline of the sample region. All the ^{32}S n,p data from the DORT XY model were divided by this 2-D model normalization factor (norm = 1.16) to put the calculations on a consistent basis with the measured ^{32}S n,p reaction rate data. The normalization procedure used here is quite consistent with previous studies involving 2-D models of real 3-D systems.⁵⁻⁶

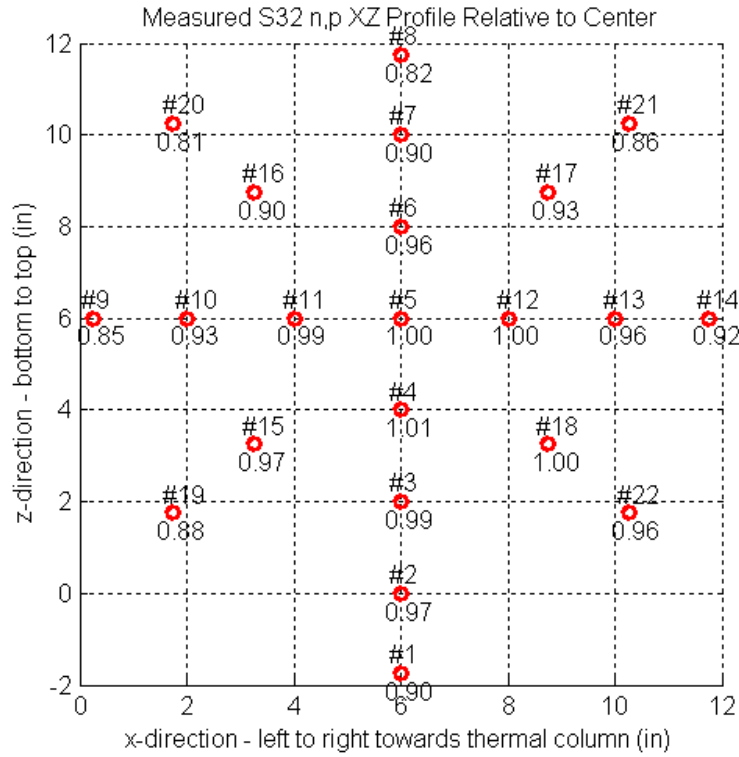


Fig. 5 Measured ^{32}S n,p normalized reaction rate distribution in the XZ plane.

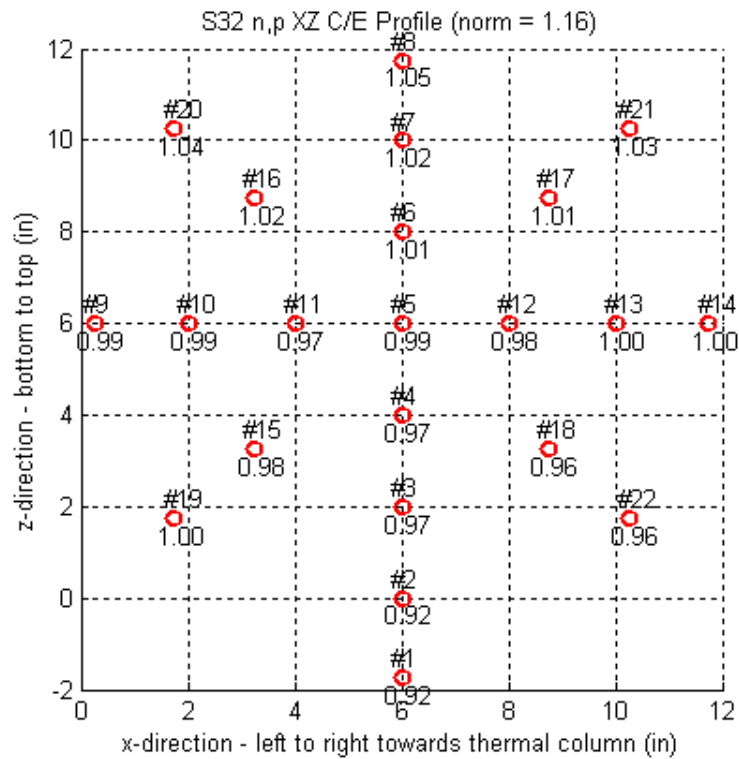


Fig. 6 ^{32}S n,p C/E distribution in the XZ plane.

A 2-D spline fit was used to extract computed data at the same x,y points as the measured data. The numerical results (reactions/second per atom) are given in the next to last column of Table 1. These computed values divided by the corresponding experimental values give the C/E ratio in the last column of the table. As apparent, once the overall bias of 1.16 is removed, the calculations and measurements have good agreement, with an average C/E = 0.99±0.03. There is a slight skew in the axial C/E profile, however, with a slight over prediction at the top and an under prediction near the bottom. These C/E trends can easily be seen in Fig. 6, which gives a composite C/E map for the 22 experimental locations in the XZ plane. Overall, however, the simplified 2-D computations did remarkably well in predicting the ³²S n,p distributions.

One additional point of interest to note before leaving the discussion of the fast flux uniformity in the XZ plane concerns the adequacy of the ³²S n,p reaction rate in predicting this quantity. In the design of the FNI, several different parameters were used as indicators of the fast neutron flux, including the $\phi > 0.01$ MeV, the $\phi > 0.1$ MeV, the $\phi > 1$ MeV, and the 1 MeV equivalent flux. The 1 MeV equivalent flux for silicon displacement was used as one of the primary indicators and it is formally defined⁷ as

$$\phi_{eq}(E_o) = \frac{\int_{E_{min}}^{E_{max}} K_D(E)\phi(E)dE}{K_D(E_o)} \quad (2)$$

where $K_D(E)$ is the neutron displacement kerma for silicon as a function of energy, E_o is the reference energy of interest, and E_{min} and E_{max} specify the energy range for significant atomic displacement in silicon. Reference 7 suggests the use of 0.01 MeV and 18 MeV as limits for the energy range of interest and E_o is usually 1 MeV. The energy-dependent kermas used to evaluate eqn. (2) were obtained from the BUGLE-96 library,⁸ since the 47-group neutron energy structure in BUGLE-96 is identical to the energy bins chosen for this study.¹

As an example of the typical differences seen in these quantities, Table 2 contains the raw computed values of these four “fast flux” indicators averaged over the sample region for the XY DORT model (with no sample present). Thus, depending on one’s definition of the “fast flux”, this quantity for the FNI could be as low as 0.5×10^{11} or as high as 2.6×10^{11} neutrons/cm²-s. Clearly, one must define exactly what is meant by the term “fast flux”.

Table 2 Computed fast flux indicators in FNI sample region.

Fast Flux Indicator	Calculated Value (n/cm²-s)
Flux > 0.01 MeV	2.55E+11
Flux > 0.1 MeV	1.83E+11
Flux > 1 MeV	5.08E+10
1 MeV Equivalent Flux	1.39E+11

The ^{32}S n,p reaction rate is often used as an experimental indicator of the fast flux since the decay rate of the ^{32}P reaction product is easy to measure. However, as mentioned earlier, the ^{32}S n,p reaction is only sensitive over the very high end of the fast energy range (2-7 MeV). Sometimes the ^{115}In n,n' reaction is also used, since it is sensitive over a somewhat broader range. Figure 7 illustrates the energy dependence of these experimental indicators by showing the normalized spectra for the $\phi > 0.1$ MeV and 1 MeV equivalent flux indicators compared to the ^{32}S n,p and ^{115}In n,n' normalized reaction rate spectra. The sum of all the group values for each of these spectra adds to unity, which allows one to easily visualize the dominant energy range associated with each indicator. Thus, we see that, although the easily measured reactions such as ^{32}S n,p and ^{115}In n,n' do relate to the desired $\phi > 0.1$ MeV and 1 MeV equivalent flux "fast flux" indicators, they certainly do not represent a perfect match. In fact, for the current case, the measured ^{32}S n,p reaction rate only covers a small portion of the energy range of interest.

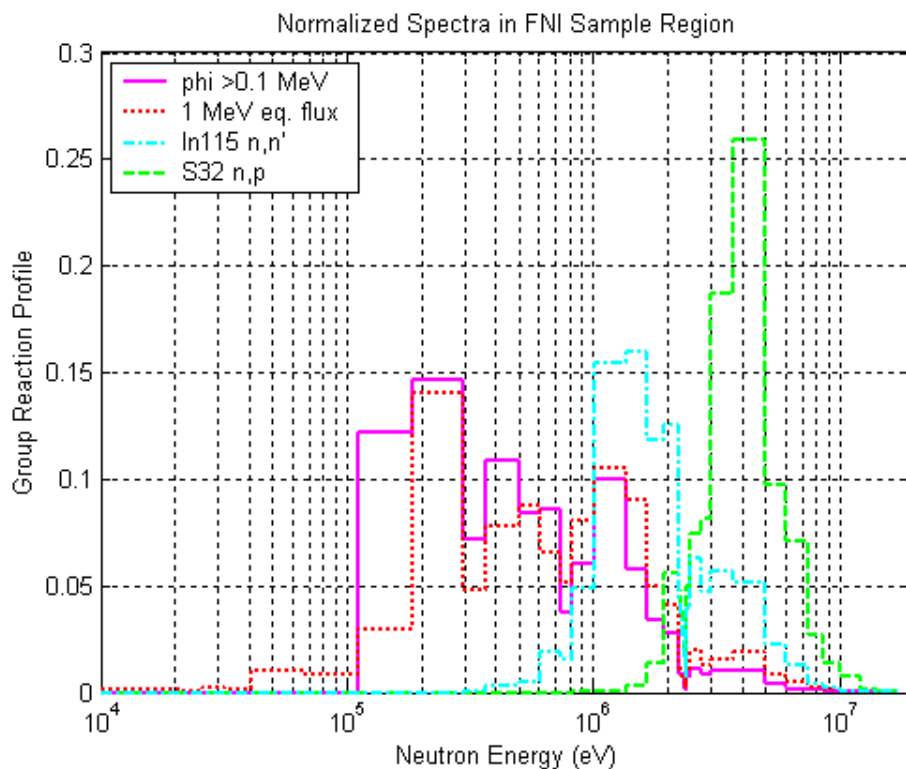


Fig. 7 Spectral distribution for several "fast flux" indicators.

The reason for the above discussion is related to the fact that the measured ^{32}S n,p reaction rate distribution shown in Fig. 5 just barely meets the design criteria of $\pm 10\%$ variation over the sample area. Based on the above arguments, however, this does not necessarily mean that the 1 MeV equivalent flux distribution will have the same variability. In fact, based on calculational evidence, it appears that the ^{32}S n,p reaction rate profile may be a relatively poor indicator of the uniformity of the 1 MeV equivalent flux, since it is only sensitive to the very high end of the energy spectrum. The calculated data show that, when more of the energy spectrum is included, the spatial distribution becomes more uniform, due probably to the scattering of very high energy neutrons over a larger spatial domain.

This observation is illustrated in the series of four contour plots given in Figs. 8-11. This sequence shows the spatial distribution of the same four “fast flux” indicators as highlighted in Fig. 7. Focusing on the spatial dependence of these indicators, it is obvious that Fig. 8, which contains the high energy ^{32}S n,p reaction rate profile, shows the largest spatial variation over the 12”x12” XZ sample area. This profile is very similar to the measured distribution displayed in Fig. 5, and they both show a maximum-to-minimum variation of about 20% over the sample region. The other three “fast flux” indicators, however, show only a 10% max-to-min variation.

Clearly each indicator has its own unique profile, but as seen here, when a larger portion of the high energy region is included, the spatial variation is reduced relative to that observed for the ^{32}S n,p reaction. In particular, for the 1 MeV equivalent flux indicator shown in Fig. 10, the >0.90 normalized contours cover most of the 12”x12” sample area. Thus, for the real indicator of interest, most of the sample area satisfies a $\pm 5\%$ variability constraint.

In summary, although direct experimental evidence is not available, it appears that the 1 MeV equivalent flux distribution in the XZ plane will easily meet the original design criteria ($\pm 10\%$ variation). The computational information displayed in Figs. 7-11, plus the relatively good agreement between the calculated and measured ^{32}S n,p reaction rate distribution (as seen in Fig. 6), supports this conclusion. Since a direct measurement of the 1 MeV equivalent flux at several points within the sample region is not feasible, Fig. 10 will be used as the current best estimate of the spatial behavior of this property over the sample region in the XZ plane.

Spectrum Measurement via Foil Activation

Once a uniform spatial distribution in the XZ plane was established, an effort was made to approximate, experimentally, an absolute value for the 1 MeV equivalent flux within the FNI sample region. The procedure used here is a simple alternative to the approach described in Ref. 7. It involves the use of measured activities for several foils that are sensitive over different energy regions, plus the use of spectrum-averaged cross sections for each reaction of interest. The ratio of the measured reaction rate per atom and the microscopic reaction cross section then gives an indirect measure of the energy-integrated neutron flux present during the irradiation.

Since the measured saturated activity, RR_m , is given by

$$RR_m = \int_{\Delta E} \sigma(E)\phi(E)dE \quad (3)$$

and the calculated spectrum-averaged cross section, $\bar{\sigma}_c$, is defined as

$$\bar{\sigma}_c = \frac{\int_{\Delta E} \sigma(E)\phi(E)dE}{\int_{\Delta E} \phi(E)dE} = \frac{RR_c}{\phi_c} \quad (4)$$

where ϕ_c is the calculated flux, we see that the “measured flux”, ϕ_m , can be estimated by

$$\phi_m = \frac{RR_m}{\bar{\sigma}_c} \quad (5)$$

The only assumption here is that the calculated spectrum-averaged cross section is a reasonable estimate of the real thing -- which is usually a valid approximation.

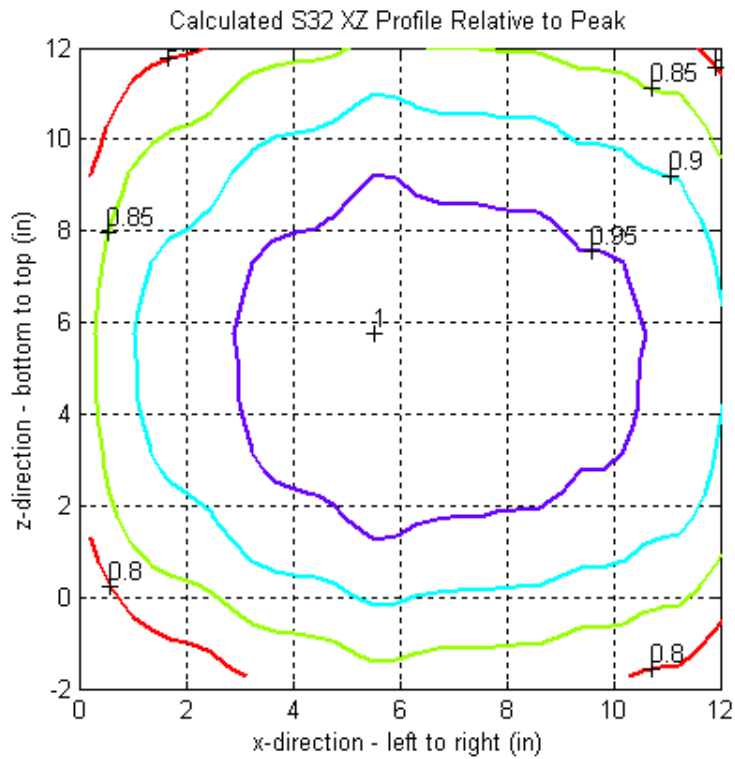


Fig. 8 Calculated ^{32}S n,p reaction profile in the XZ plane.

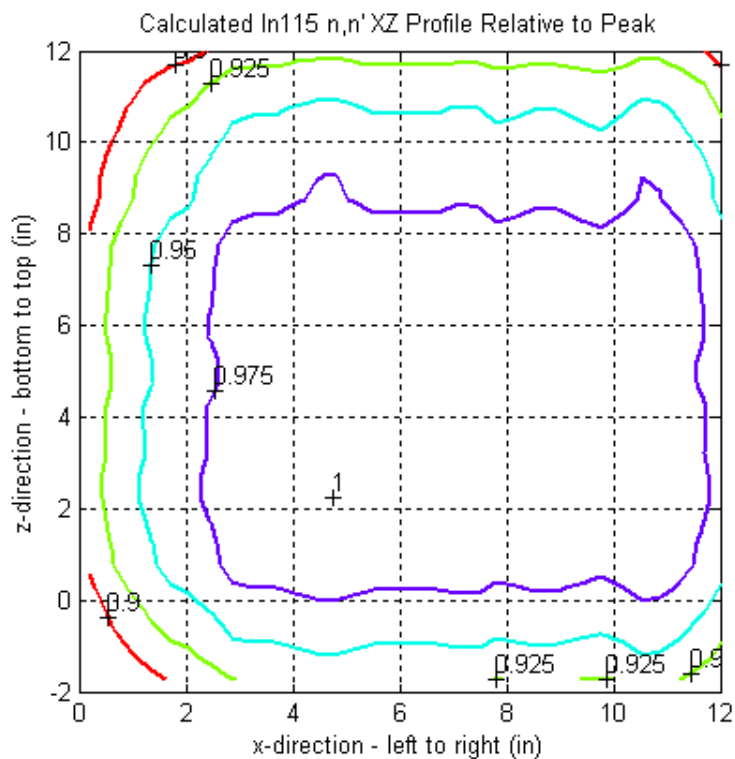


Fig. 9 Calculated ^{115}In n,n' reaction profile in the XZ plane.

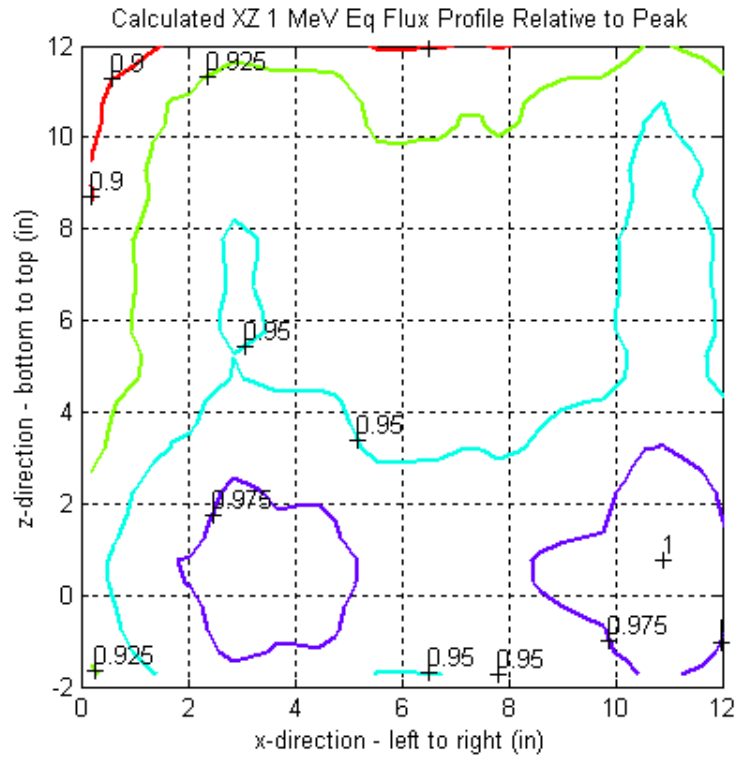


Fig. 10 Calculated 1 MeV equivalent flux profile in the XZ plane.

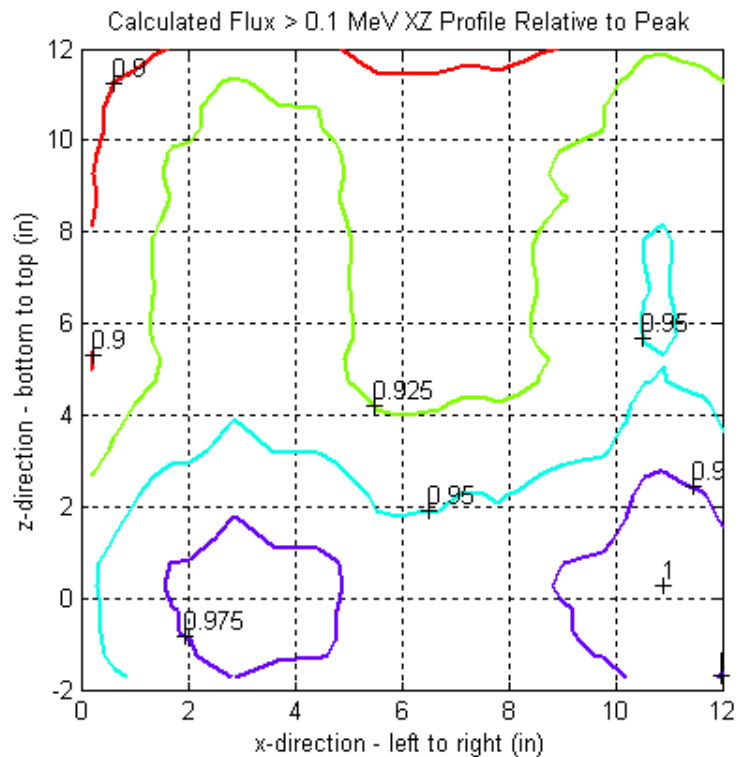


Fig. 11 Calculated $\phi > 0.1$ MeV profile in the XZ plane.

With several estimates of ϕ_m from different activation foils, one can obtain an overall estimate of the average measured flux, $\bar{\phi}_m$. In addition, an uncertainty estimate can also be established by determining the relative standard deviation about the mean of the measured flux.

The energy interval of interest, ΔE , for the above integrals was chosen to be consistent with the E_{\min} to E_{\max} range used in the definition of the 1 MeV equivalent flux given in eqn. (2). Thus, all the spectrum-averaged cross sections and the measured fluxes, given by eqns. (4) and (5), are determined over the range of 0.01 MeV to 18 MeV.

To get a measured value of the 1 MeV equivalent flux from the measured $\phi > 0.01$ MeV, we simply multiply ϕ_m from eqn. (5) by the relative damage factor, RDF, or

$$\phi_{eq} = RDF * \phi_m \quad (6)$$

where the RDF is given in Ref. 7 as

$$RDF = \frac{\int_{E_{\min}}^{E_{\max}} K_D(E)\phi(E)dE}{K_D(E_o)\int_{E_{\min}}^{E_{\max}} \phi(E)dE} = \frac{\phi_{eq}(E_o)}{\phi_T} \quad (7)$$

Here ϕ_T is the total energy-integrated flux over the interval of interest. The RDF is often used as a convenient measure for characterizing the spectrum of a particular facility. It represents the fluence of 1 MeV neutrons required to produce the same displacement kerma in silicon as a unit fluence of neutrons of spectral distribution $\phi(E)$.

The first part of eqn. (7) was evaluated using the computed data from the DORT XY model averaged over the full sample area with a resultant RDF of 0.544. The ϕ_T in eqn. (7) is the same as the ϕ_m from eqn. (5) that is measured as part of the foil activation experiments. Thus, putting together the calculated RDF from eqn. (7) and the measured flux from eqn. (5) gives the desired “measured value” of the 1 MeV equivalent flux as indicated in eqn. (6).

To actually measure the 1 MeV equivalent flux using the above procedure, a set of foils were positioned on an aluminum sheet as shown in Fig. 12 and placed in the center of the FNI sample area. The foil set had 7 foils for measuring the fast portion of the neutron spectrum (In, U, Th, Ti, Ni, Zn, and Mg), two foils for measuring the epithermal and thermal flux components (Sc and Au), and three non-reversible temperature crayons (at 125 F, 150 F, and 175 F) to get an idea of the actual temperature inside the sample canister.

Of interest here is the set of 7 foils for the characterization of the fast spectrum, specifically the 1 MeV equivalent flux. Unfortunately, however, the necessary multigroup activation cross sections for the ^{64}Zn n,p and ^{24}Mg n,p reactions are not available in the cross section library used for the current analysis,¹ so only raw experimental data are reported for these reactions (no computational analysis is possible at this time). Also, a direct ^{32}S n,p measurement was inadvertently omitted from the foil set. However, as seen in subsequent results, an attempt was made to include this reaction in the measurement of the 1 MeV equivalent flux by incorporating approximate experimental data from another, slightly different experiment (see previous section).

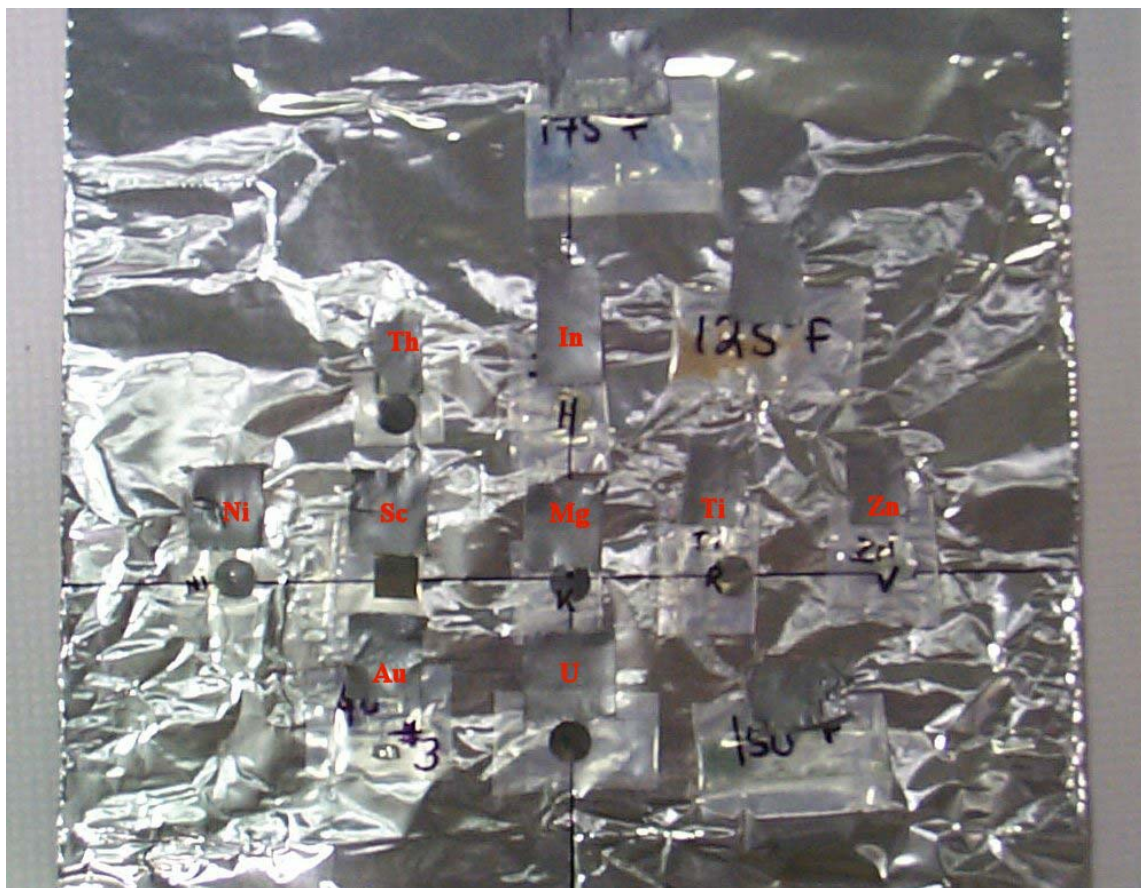


Fig. 12 Placement of foils for spectrum characterization in FNI.

The samples shown in Fig. 12 were irradiated at an indicated power level of 1 MW (really only 900 KW) for four hours with a mid-cycle 180° rotation of the FNI sample canister. After an appropriate cool-down time, the saturated activities (reactions/second per atom) were measured, with the raw experimental results given in the first part of Table 3. These data were divided by the UMLRR calibration bias of 0.90 to account for the difference in the actual power level and the indicated level. Thus, the values in the 3rd column of Table 3 represent the measured reaction rate, RR_m in eqns. (3) and (5), for an actual power level of 1 MW.

Also included in Table 3 are the computed values for the individual reaction rates and the calculated-to-experimental ratios (C/Es). As apparent, the calculated reaction rate is higher than the measured value for each case, with the C/E varying from about 1.3 to 1.5 in most cases. Because of the estimated nature of the ^{32}S n,p reaction (this value in Table 3 was estimated from a different experiment), two average C/E values were computed, with and without this reaction included. In both cases, however, the average bias in the calculation is near 40%, with a somewhat reduced uncertainty if the ^{32}S n,p reaction is omitted.

The last section of Table 3 includes the computed spectrum-averaged cross section, $\bar{\sigma}_c$, and the “measured” $\phi > 0.01$ MeV, ϕ_m , from eqn. (5). This latter value, for each of the individual foils with available reaction cross sections, was multiplied by the relative damage for the FNI (RDF = 0.544) to give an estimate of the “measured” 1 MeV equivalent flux as described in eqns. (6) and (7). Again, two averages were calculated, depending on whether or not the ^{32}S n,p reaction is

included, with a measured 1 MeV flux level of about 10^{11} n/cm²-s. This value is at the lower limit that was set for the desired operation of the FNI.

The experimental values are also compared to the computed 1 MeV equivalent flux, with C/Es in the range of 1.35 - 1.42. Again, the calculated-to-experimental bias is not a concern, since a 2-D normalization is always needed for real 3-D systems that are modeled with simplified 2-D geometries.

Also of interest is the uncertainty in the measured 1 MeV equivalent flux. There are 5 or 6 somewhat independent measures of this quantity, depending on whether or not the estimate from the ³²S n,p reaction is used. The relative standard deviation, however, is a little larger than desired, with values of about $\pm 7\%$ and $\pm 14\%$. This uncertainty can be attributed to several factors, such as the counting statistics, variations in measurement location, uncertainties in the computed spectrum-averaged cross section and RDF, and the overall small number of measurements. Hopefully, including the ⁶⁴Zn n,p and ²⁴Mg n,p reactions and a more consistent estimate of the ³²S n,p reaction rate in future analyses will help reduce this uncertainty to under $\pm 5\%$ (an uncertainty of less than 5% was the original goal).

In summary, a measurement of the 1 MeV equivalent flux within the empty FNI sample canister gives a value near 10^{11} n/cm²-s with an uncertainty around 10%. This value is only about 35-40% lower than the value predicted from the base XY DORT computation model. Thus again, we see that the 2-D models generated as part of the FNI design effort were indeed sufficient as a design and analysis tool for this project.

Miscellaneous Measurements

In addition to the experiments described above, a series of other miscellaneous parameters were also measured as part of a full characterization program for the new FNI facility. This section briefly describes some of these additional tests.

Low Energy Neutron Flux

Neutron capture in gold and scandium are often used to assess the magnitude of the low energy portion of the neutron spectrum. In particular, the Au n, γ reaction varies with neutron energy or velocity, v , with a nearly $1/v$ behavior below 1 eV and a large broad resonance near 5 eV. Because of the low energy resonance, gold foils are often cadmium covered to eliminate the thermal energy component of the reaction rate (below 1 eV). By comparing the measured activity of the bare and Cd-covered gold foils, one can focus on only the thermal neutron component below 1 eV. The Sc n, γ reaction also has a $1/v$ cross-section profile below about 100 eV and a fairly wide resonance region from 500 eV up to almost 100 keV. Thus, this reaction should cover most of the thermal and epithermal energy range (above thermal and below fast).

Combinations of gold (bare and Cd-covered) and scandium foils were used on various occasions to try to measure the low energy neutron flux in the FNI canister region. For example, as apparent in Fig. 12, this fast flux experiment also included bare Au and Sc foils sets. Earlier measurements also included both bare and Cd-covered gold foils.

Table 3 Measured and computed data for determining the 1 MeV equivalent flux.

Reaction	Measured Reaction Rate*	Measured Reaction Rate for 1 MW	Calculated Reaction Rate for 1 MW	C/E		Average Cross Section (b) ***	Measured $\phi > 0.01$ MeV		Measured 1 MeV Eq. Flux	
				with ^{32}S	no ^{32}S		with ^{32}S	no ^{32}S	with ^{32}S	no ^{32}S
^{115}In n,n'	7.31E-15	8.12E-15	1.08E-14	1.33		4.23E-02	1.92E+11		1.05E+11	
^{238}U n,f	9.29E-15	1.03E-14	1.63E-14	1.58		6.39E-02	1.62E+11		8.79E+10	
^{232}Th n,f	2.52E-15	2.80E-15	3.80E-15	1.36		1.49E-02	1.88E+11		1.02E+11	
^{47}Ti n,p	4.81E-16	5.35E-16	7.97E-16	1.49		3.12E-03	1.71E+11		9.32E+10	
^{58}Ni n,p	2.22E-15	2.46E-15	3.43E-15	1.39		1.34E-02	1.83E+11		9.98E+10	
^{64}Zn n,p	6.84E-16	7.60E-16								
^{24}Mg n,p	2.67E-17	2.97E-17								
^{32}S n,p **	1.56E-15	1.73E-15	1.99E-15	1.15		7.35E-03	2.36E+11		1.28E+11	
				with ^{32}S	no ^{32}S		with ^{32}S	no ^{32}S	with ^{32}S	no ^{32}S
			Ave C/E	1.38	1.43	Ave Flux	1.89E+11	1.79E+11	1.03E+11	9.75E+10
			Std Dev	0.15	0.10	Std Dev	2.57E+10	1.26E+10	1.40E+10	6.88E+09
			Rel Std Dev (%)	10.7	7.3	Rel Std Dev (%)	13.6	7.0	13.6	7.0
							C/E 1 MeV Flux		1.35	1.42

* Reaction rates have units of reactions/second per atom.

** The ^{32}S n,p data are estimated from a different physical experiment.

*** All the average cross sections are based on the flux above 0.01 MeV.

As an illustration, the specific reaction rate data from the experimental arrangement in Fig. 12, along with the raw calculational results from the DORT XY model are summarized in Table 4. The most obvious result here is that the calculations seriously over-predicted both the epithermal and thermal neutron flux components. Although we don't really know why this occurred (requires further study), the more important result is that the calculated thermal neutron flux was already quite low -- easily meeting the original goal of a 10:1 or greater fast-to-thermal flux ratio. Thus, the experimental results indicate an even lower thermal flux than expected.

Table 4 Measured and computed data for the low energy component of the neutron flux.

Reaction	Measured Reaction Rate*	Measured Reaction Rate for 1 MW	Calculated Reaction Rate for 1 MW	C/E
$^{197}\text{Au } n,\gamma$	1.51E-12	1.67E-12	1.90E-11	11.3
$^{45}\text{Sc } n,\gamma$	3.57E-14	3.97E-14	1.38E-13	3.47

* Reaction rates have units of reactions/second per atom.

To highlight this result, Table 2 from Ref. 1 is reproduced here as Table 5 -- the reader is referred to Ref. 1 for a more detailed description of this table. Of immediate interest for the current discussion is the fact that the calculated fast-to-thermal flux ratio given by $1.83 \times 10^{11} / 4.85 \times 10^9 \approx 38$ is probably low by as much as a factor of 10. Thus, this says that the thermal flux ($\phi < 1$ eV) is extremely low within the FNI canister. The experimental results in Table 4 also suggest that the calculated epithermal flux given in Table 5 is probably too high by at least a factor of 3. Thus, it appears that the FNI is indeed predominantly a facility for fast neutron irradiations.

The observation that the thermal neutron flux is very low was reinforced in a separate measurement made early in the testing program. In this early test, both bare and Cd-covered foils were placed in an empty FNI canister and irradiated for a short time. Upon measurement, the Cd-covered foil had a slightly higher saturated activity than the bare foil. This rather surprising result was corroborated with a computational simulation of the same setup. This result, although a little confusing at first, simply indicates that the thermal neutron flux within the FNI canister is indeed very low -- in fact, it is too low to measure using the Cd-covered foil activation method.

Gamma Dose Rate

Measurements of the gamma dose rate within the new FNI facility have also been made. A calibrated high-range underwater survey meter (Technical Associates Model CP-MU) was used to do both wet and dry measurements. The CP-MU consists of a small ionization chamber, 60 ft of coaxial cable, and associated electronics, including an indicating meter. An accuracy of $\pm 15\%$ is quoted by the manufacturer for the full-scale reading on the CP-MU. The ionization chamber was positioned at the sample irradiation location. For the dry test, the ionization chamber was placed in a dry canister and the coaxial cable was routed to the survey meter via a conduit port in the canister lid. A compression fitting between the cable and lid port provided a leak-tight seal.

**Table 5 Raw calculated results for in-core location D2 and the new ex-core FNI facility.
(directly from Table 2 of Ref. 1)**

Parameter of Interest	Radiation Basket D2	FNI Sample
Broad Group Fluxes (n/cm²-sec)		
Fast Flux > 0.1 MeV	3.26E+12	1.83E+11
Epithermal Flux	3.42E+12	2.45E+11
Thermal Flux < 1 eV	1.14E+13	4.85E+09
Total Neutron Flux	1.81E+13	4.33E+11
Total Gamma Flux	2.95E+13	5.05E+10
Additional Fast Flux Characterization		
Fast Flux > 1 MeV	1.72E+12	5.08E+10
Fast Flux > 0.01 MeV	4.02E+12	2.55E+11
1 MeV Equiv. Flux	3.08E+12	1.39E+11
RDF	0.77	0.55
Energy Deposition Rates (Krad/hr)		
Neutrons in Air	2.58E+04	1.38E+02
Neutrons in Silicon	9.37E+02	3.20E+01
Gammas in Air	3.50E+04	4.40E+01
Gammas in Silicon	3.74E+04	4.62E+01

The gamma dose rates from the two separate measurements are compared to computed values in Table 6. Again, the measured data have been normalized to an effective power level of 1 MW for direct comparison to the computed values. The wet measured dose rate of 410 Krad/hr is associated with the middle of the water-filled FNI sample region (no canister present). In contrast, the measured gamma dose rate in the center of the dry empty canister was only 110 Krad/hr. This dry configuration is more typical of the gamma environment that will be present during actual use of the facility (i.e. with experimental samples placed within the dry FNI canister). One should note, however, that a nominal dry dose rate of 110 Krad/hr does exceed the original design goal of < 100 Krad/hr.

Also, as apparent from Table 6, both the wet and dry gamma dose rates were under predicted within the DORT XY computational model. This result was somewhat unexpected, especially since the low energy neutron flux was over predicted by a large factor. This calculated versus experimental discrepancy has not been explained at present and, since it does not really impact operation of the FNI, it will be left for further analysis and resolution at a later date.

Table 6 Measured and calculated gamma dose rates (Krad/hr) in the FNI sample region.

Location	Measured Value	Calculated Value
Water-filled sample region	410	300
Empty FNI canister	110	50

Temperature Level

As mentioned previously, a set of three non-reversible temperature crayons with melting points of 125 F, 150 F, and 175 F were included as part of one of the spectrum characterization experiments. The goal here was to get an idea of the temperature level inside an empty sample canister. Since none of the crayons showed any indication of melting, we know that the operational temperature of an empty FNI canister is less than 125 F with the reactor at 1 MW for four hours. Of course, energy deposition within a large sample over time will tend to increase the temperature via internal heating, but this initial measure shows that the sample-free environmental temperature, at least, is quite reasonable.

Blade Worth Distribution

Although not directly related to the FNI facility, a series of additional operational evaluations were also made for the post-FNI reactor configuration. Of particular interest was a full blade worth calibration for the new core layout, including the ex-core FNI, the in-core Pb-void boxes, and the final placement of the full and partial fuel elements. Table 4 from Ref. 1 is reproduced here as Table 7 to show the measured and calculated blade worths. Of importance is the good prediction of the blade worth distribution, with Blade #4 having the largest total worth. This good agreement suggests that the in-core power and fission source distributions determined from the VENTURE XY model are probably quite representative of those in the actual system. Since this XY fission source distribution was used for all the XY DORT models for the design and characterization of the FNI, this comparison establishes some credibility with the base core model. Previous tests of the base VENTURE and DORT XY models⁹ have also validated the overall modeling procedures used at UMass-Lowell.

**Table 7 Comparison of measured and calculated blade worths.
(directly from Table 4 of Ref. 1)**

Parameter	Measured % $\Delta k/k$	Calculated % $\Delta k/k$
Blade 1 Worth	2.82	2.87
Blade 2 Worth	2.19	2.14
Blade 3 Worth	3.19	2.99
Blade 4 Worth	3.93	3.96

Summary/Future Work

The initial testing of the new ex-core fast neutron irradiator (FNI) at the UMass-Lowell research reactor (UMLRR) is now complete and the new facility is now available for routine use. The primary goal of the initial measurement program was to characterize the overall radiation environment within the empty FNI canister. The measured data indicate that the 1 MeV equivalent flux level is about 10^{11} n/cm²-s (see Table 3) and that the fast fluence rate distribution is relatively uniform over the 12"x12"x6" sample volume (see Figs. 5, 8, and 10). In addition, the thermal and epithermal components of the neutron spectrum are very low (see Tables 4 and 5). These characteristics either meet or exceed the original design specifications for the FNI facility. The measured gamma dose of 110 Krad/hr, however, did exceed the design goal of < 100 Krad/hr by a small amount. Overall, however, the new facility does indeed provide a relatively uniform fast fluence rate with a low thermal neutron and gamma ray background -- thus providing the desired environment for fast neutron irradiations within a relatively large sample volume.

Of course, another important focus of the initial experimental program was to provide measured data to help verify and validate the models and methods used during the design of the FNI. Some initial comparisons of several measured and computed parameters are given here, with overall good agreement with the prediction of the fast neutron flux indicators. However, the computational models did not do as well with the prediction of the thermal and epithermal neutron fluxes and the estimation of the gamma dose rate. Further study is needed to resolve the observed discrepancies for these quantities. Overall, however, it appears that the 2-D VENTURE and DORT models used here were indeed sufficient for use as a design tool -- since the final product does appear to perform as desired.

Clearly additional experimental characterization will be performed as the FNI is used for a variety of applications. Data from the current study suggests, however, that the ¹¹⁵In n,n' reaction may be a better indicator of the 1 MeV equivalent fluence -- so it is recommended that future evaluations use indium foils rather than sulfur tablets. Also, as time and funding permits, additional computer modeling should be initiated to try to resolve some of the differences observed between the as-built system and the simplified 2-D models used here. One enhancement, in particular, that may help answer many questions and also provide more robust analytical capability to support future FNI operations is a detailed 3-D model of the reactor and ex-core FNI facility. This would require a substantial effort, however, so time and funding issues will need to be resolved before we can go down this path.

References

1. J. R. White, et. al., "Design and Initial Testing of an Ex-Core Fast Neutron Irradiator for the UMass-Lowell Research Reactor," 2002 ANS Radiation Protection and Shielding Topical Conference, Santa Fe, NM (April 2002).
2. "VENTURE-PC - A Reactor Analysis Code System," Radiation Safety Information Computational Center, CCC-654 (1997).
3. "DOORS3.1 - One, Two, and Three Dimensional Discrete Ordinates Neutron/Photon Transport Code System," Radiation Safety Information Computational Center, CCC-650 (1996).

4. "Proposed Technical Specifications for the University of Massachusetts Lowell Reactor with Low Enrichment Fuel," submitted to the NRC for conversion of the UMass-Lowell Research Reactor (May 1993).
5. J. R. White, et. al., "Calculational Support for the Startup of the LEU-Fueled UMass-Lowell Research Reactor," Advances in Reactor Physics and Mathematics and Computation, Pittsburgh, PA (May 2000).
6. J. R. White, et. al., "Preliminary Characterization of the Irradiation Facilities within the LEU-Fueled UMass-Lowell Research Reactor," Advances in Reactor Physics and Mathematics and Computation, Pittsburgh, PA (May 2000).
7. "Characterizing Neutron Energy Fluence Spectra in Terms of an Equivalent Monoenergetic Neutron Fluence for Radiation-Hardness Testing of Electronics," ASTM Standard Practice E722-85 (1985).
8. "BUGLE-96 - Coupled 47 Neutron, 20 Gamma-Ray Group Cross Section Library from ENDF/B-VI for LWR Shielding and Pressure Vessel Dosimetry Applications," Radiation Safety Information Computational Center, DLC-185 (1996).
9. "Report on the HEU to LEU Conversion of the University of Massachusetts Lowell Research Reactor," submitted to the NRC in fulfillment of Amendment No. 12 to License No. R-125 (April 2001).